CHAPTER 3

VERTICAL SIDE SHAER AND PILE POINT TIP RESISTANCE OF A PILE / SHAFT IN CLAY

3.1 INTRODUCTION

The primary focus of this chapter is the evaluation of the vertical side shear induced by the vertical displacement accompanying the deflection of a laterally loaded shaft. The prediction of the vertical side shear of a laterally loaded shaft is not feasible unless a relationship between the vertical shaft displacement and the associated shear resistance is first established. The most common means to date is the t-z curve method proposed by Seed and Reese (1957). The associated curves were developed using experimental data from the vane shear test to represent the relationship between the induced shear stress (due to load transfer) and vertical movement (z) along the side of the pile shaft (Fig. 3-1). Other procedures are available to generate the t-z curve along the pile shaft (Coyle and Reese 1966; Grosch and Reese 1980; Holmquist and Matlock 1976 etc.). Most of these procedures are empirical and based on field and experimental data. Others are based on theoretical concepts such as the methods presented by Randolph and Worth (1978), Kraft et al. (1981) in addition to the numerical techniques adopted by Poulos and Davis (1968), Butterfield and Banerjee (1971), and the finite element method.

It should be noted that any developed t-z relationship is a function of the pile/shaft and soil properties (such as shaft diameter, cross section shape and material, axial stiffness, method of installation and clay shear stress-strain-strength). This requires the incorporation of as many soil and pile properties as useful and practical in the suggested analysis.

Coyle and Reese (1966) presented an analytical method to assess the load transfer relationship for piles in clay. The method is addressed in this chapter and requires the use of a t-z curve such as those curves suggested by Seed and Reese (1957), and Coyle and Reese (1966) shown in Figs. 3-1 and 3-2. However, the t-z curve presented by Seed

and Reese (1957) is based on the vane shear test, and the t-z curve developed by Coyle and Reese (1966) is based on data obtained from a number of pile load tests from the field (Fig. 3-2).

The current chapter presents a procedure for evaluating the change in the axial load with depth for piles in clay called "friction" piles since most of the axial load is carried by the shaft (as opposed to the pile point). The load transfer mechanism presented by Coyle and Reese (1966) is used in the proposed analysis in association with the t-z curve developed herein. In fact, the axially loaded pile analysis is just a means to develop the nonlinear t-z curves for clay that will be used later to assess the vertical side shear resistance of a laterally loaded large diameter shaft undergoing vertical movement at its edges as it rotates from vertical.

3.2 LOAD TRANSFER AND PILE SETTLEMENT

In order to construct the load transfer and pile-head movement in clay under vertical load, the t-z curve for that particular soil should be assessed. The load transferred from shaft skin to the surrounding clay soil is a function of the diameter and the surface roughness of the shaft, clay properties (cohesion, type of consolidation and level of disturbance) in addition to the shaft base resistance. The development of a representative procedure allows the assessment of the t-z curve in soil (sand and/or clay) that leads to the prediction of a nonlinear vertical load-settlement response at the shaft head. Such a relationship provides the mobilized shaft-head settlement under axial load and the ration of load displacement or vertical pile head stiffness.

The procedure developed by Coyle and Reese (1966) to assess the load-settlement curve is employed in this section. However, such a procedure requires knowledge of the t-z curves (theoretical or experimental) that represent the load transfer to the surrounding soil at a particular depth for the pile movement (z).

The following steps present the procedure that is employed to assess the load transfer and pile movement in clay soil:

1. Based on Skempton assumptions (1951), assume a small shaft base resistance, q_P (small percentage of q_{net} = 9 C).

$$q_P = 9\ C_m = 9\ C\ SL = SL\ q_{net} \quad (3\text{-}1)$$

$$Q_P = q_P\ A_{base} = SL\ q_{net}\ A_{base} \quad (3\text{-}2)$$

C is equal to the clay undrained shear strength, S_u. A_{base} is the area of the pile tip (shaft base).

2. Using the SL evaluated above and the stress-strain relationship presented in Chapter 5 [Norris (1986) and Ashour et al. (1998)], compute the induced axial (deviatoric) soil strain, ε_P and the shaft base displacement, z_P

$$z_P = \varepsilon_P\ B \quad (3\text{-}3)$$

where B the diameter of the shaft base. See Section 3-3 for more details.

3. Divide the pile length into segments equal in length (h_s). Take the load Q_B at the base of the bottom segment as (Q_P) and movement at its base (z_B) equal to (z_P). Estimate a midpoint movement for the bottom segment (segment 4 as seen in Fig. 3-3). For the first trial, the midpoint movement can be assumed equal to the shaft base movement.

4. Calculate the elastic axial deformation of the bottom half of this segment,

$$z_{elastic} = \frac{Q_B h_s / 2}{E A_{base}} \quad (3\text{-}4)$$

The total movement of the midpoint in the bottom segment (segment 4) is equal to

$$z = z_T + z_{elastic} \quad (3\text{-}5)$$

5. Based on the soil properties of the surrounding soil (S_u and ε_{50}), use a Ramberg-Osgood formula (Eqn. 3-6) to characterize the backbone response (Richart 1975).

$$\frac{z}{z_r} = \frac{\gamma}{\gamma_r} = \frac{\tau}{\tau_{ult}} \left[1 + \beta \left(\frac{\tau}{\tau_{ult}} \right)^{R-1} \right] \qquad (3\text{-}6)$$

z = total midpoint movement of a pile/shaft segment

γ = average shear strain in soil adjacent to the shaft segment

τ = average shear stress in soil adjacent to the shaft segment

γ_r is the reference strain, as shown in Fig. 3-4, and equals to G_i / τ_{ult}

z_r = shaft segment movement associated to γ_r

ε_{50} = axial strain at SL = 0.5 (i.e. $\sigma_d = S_u$). ε_{50} can be obtained from the chart provided in Chapter 5 using the value of S_u.

β and R-1 are the fitting parameters of the a Ramberg-Osgood model given in Eqn. 3-7. These parameters are evaluated in section 3.2.1.

6. Using Eqn. 3-6 which is rewritten in the form of Eqn. 3-7, the average shear stress level ($SL_t = \tau / \tau_{ult}$) in clay around the shaft segment can be obtained iteratively based on movement z evaluated in Eqn. 3-5.

$$\frac{z}{z_r} = \frac{\gamma}{\gamma_r} = SL_t \left[1 + \beta (SL_t)^{R-1} \right] \qquad \text{(Solved for } SL_t\text{)} \qquad (3\text{-}7)$$

7. Shear stress at clay-shaft contact surface is then calculated, i.e.

$$\tau = SL_t \, \tau_{ult} \qquad \text{or} \qquad \tau = SL_t \, \alpha \, C \qquad (3\text{-}8)$$

where α is the ratio of C_A/C that expresses the variation in the cohesion of the disturbed clay (C_A) due to pile installation and freeze, as seen in Fig. 3-5 (DM7.2 , 1986). It should be noted that the drop in soil cohesion is accompanied by a drop in the initial shear modulus (G_i) of the clay

8. The axial load carried by the shaft segment in skin friction / adhesion (Q_s) is expressed as

$$Q_s = \pi\ B\ H_s\ \tau \tag{3-9}$$

9. Calculate the total axial load (Q_i) carried at the top of the bottom segment (i = 4).

$$Q_i = Q_s + Q_B \tag{3-10}$$

10. Determine the elastic deformation in the bottom half of the bottom segment assuming a linear variation of the load distribution along the segment.

$$Q_{mid} = (Q_i + Q_B) / 2 \tag{3-11}$$

$$z_{elastic} = \left(\frac{Q_{mid} + Q_B}{2} H_s \right) / EA = \frac{(Q_i + 3Q_B)\, H_s}{8EA} \tag{3-12}$$

11. Compute the new midpoint movement of the bottom segment.

$$z = z_P + z_{elastic} \tag{3-13}$$

12. Compare the z value calculated from step 11 with the previously evaluated estimated movement of the midpoint from step 4 and check the tolerance.
13. Repeat steps 4 through 12 using the new values of z and Q_{mid} until convergence is achieved
14. Calculate the movement at the top of the segment i= 4 as

$$z_i = z_B + \frac{Q_i + Q_B}{2} \frac{H_s}{AE}$$

15. The load at the base (Q_B) of segment i = 3 is taken equal to Q_4 (i.e. Q_{i+1}) while z_B of segment 3 is taken equal to z_4 and steps 4-13 are repeated until convergence for segment 3 is obtained. This procedure is repeated for successive segments going up until reaching the top of the pile where pile head load Q is Q_t and pile top

movement δ is z_1. Based on presented procedure, a set of pile-head load-settlement coordinate values (Q - δ) can be obtained on coordinate pair for each assumed value of Q_T. As a result the load transferred to the soil along the length of the pile can be calculated for any load increment.

16. Knowing the shear stress (τ) and the associated displacement at each depth (i.e. the midpoint of the pile segment), points on the t-z curve can be assessed at each new load.

3.3 DEVELOPED t-z CURVE RELATIONSHIP

For a given displacement (z), the mobilized shear stress (τ) at the shaft-soil interface can be expressed as a function of the ultimate shear strength (τ_{ult}) via the shear stress level (SL_t).

$$SL_t = \tau / \tau_{ult} \tag{3-14}$$

The shear displacement of the soil around the pile decreases with increasing distance from the pile wall (Fig. 3-6). Based on a model study (Robinsky and Morrison 1964) of the soil displacement pattern adjacent to a vertically loaded pile, it has been estimated (Norris, 1986) that the average shear strain, γ, within a zone of B/2 wide adjacent to the pile accounts for 75% of the shear displacement, z, as shown in Fig. 3-7. A linear shear strain, γ, in the influenced zone (B/2) can be expressed as

$$g = \frac{0.75\ z}{B/2} = \frac{1.5z}{B} \tag{3-15}$$

Therefore,

$$z = \frac{gB}{1.5} \tag{3-16}$$

As seen in Fig. 3-7 and because z is directly related to γ based on shaft diameter (Eqn.3-16), note that

$$\frac{z_{50}}{z_f} = \frac{\gamma_{50}}{\gamma_f} \tag{3-17}$$

where z_{50} and γ_{50} are the shaft displacement and the associated shear strain in the soil at $SL_t = 0.5$ (i.e. $\tau = 0.5\ \tau_{ult}$). z_f and γ_f are the shaft displacement and the associated shear strain at failure where $SL_t = 1.0$ (i.e. $\tau = \tau_{ult}$). Therefore, the variation in the shear strain (γ) occurs in concert with the variation in shaft displacement z (Fig. 3-4). It should be noted that soil shear modulus (G) exhibits its lowest value next to the pile skin and increases with distance away from the pile to reach it is maximum value (G_i) at γ and $z \cong 0$ (Fig. 3-6). Contrary to the shear modulus, the vertical displacement (z) and the shear strain (γ) reach their maximum value in the soil adjacent to the pile face and decrease with increasing radial distance from the pile.

3.3.1 Ramberg-Osgood Model for Clay

With the above mentioned transformation of the t-z curves to τ-γ curves, a Ramberg-Osgood model represented by Eqn. 3-6 can be used to characterize the t-z curve.

$$\frac{z}{z_r} = \frac{\gamma}{\gamma_r} = \frac{\tau}{\tau_{ult}} \left[1 + \beta \left(\frac{\tau}{\tau_{ult}} \right)^{R-1} \right] \tag{3-18}$$

At $\tau/\tau_{ult} = 1$ then

$$\beta = \frac{\gamma_f}{\gamma_r} - 1 \tag{3-19}$$

At $\tau/\tau_{ult} = 0.5$ and $\gamma = \gamma_{50}$, then

$$R - 1 = \frac{\log \left(\dfrac{2\,\dfrac{\gamma_{50}}{\gamma_r} - 1}{\beta} \right)}{\log (0.5)} = \frac{\log \left(\dfrac{2\,\dfrac{\gamma_{50}}{\gamma_r} - 1}{\dfrac{\gamma_f}{\gamma_r} - 1} \right)}{\log (0.5)} \tag{3-20}$$

The initial shear modulus (G_i) and the shear modulus (G_{50}) at SL = 0.5 can be determined via their direct relationship with the normal stress-strain relationship and Poisson's ratio (ν)

$$G_i = \frac{E_i}{2(1+\nu)} = \frac{E_i}{3} \qquad \nu \text{ for clay} = 0.5 \tag{3-21}$$

and

$$G_{50} = \frac{E_{50}}{2(1+\nu)} = \frac{E_{50}}{3} = \frac{S_u}{3\varepsilon_{50}} \tag{3-22}$$

As seen in Fig. 3-4,

$$\gamma_r = \frac{S_u}{G_i} = \frac{\tau_{ult}}{G_i} \tag{3-23}$$

$$\gamma_{50} = \frac{0.5\, S_u}{G_{50}} \tag{3-24}$$

The shear strain at failure (γ_f) is determined in terms of the normal strain at failure (ε_f), i.e.

$$\gamma_f = \frac{\varepsilon_f}{(1+\nu)} = \frac{\varepsilon_f}{1.5} \tag{3-25}$$

The normal stress-strain relationship of clay (σ_d - ε) is assessed based on the procedure presented in Chapter 5 that utilizes ε_{50} and S_u of clay. The initial Young's modulus of clay (E_i) is determined at a very small value of the normal strain (ε) or stress level (SL). In the same fashion, ε_f is evaluated at SL = 1 or the normal strength $\sigma_{df} = 2S_u$.

3.4 PILE TIP (SHAFT BASE) RESISTANCE IN CLAY

In regard to the pile tip resistance ($Q_T - z_T$) response, the concept of Skempton's characterization (1951) is used as follows,

$$Q_T = q_{net} A_{base} = 9 C A_{base}$$

where clay cohesion, C, represents the undrained shear strength, S_u. The stress level (SL = σ_d / σ_{df}) in clay is proportional to the pressure level (PL = q/q_{net}). Different from the strain-deflection relationship established by Skempton (1951) for strip footing ($y_{50} = 2.5 \varepsilon_{50} B$), the vertical soil strain (ε_1) beneath the base of the shaft is expressed as

$$\varepsilon_1 = \frac{\Delta\sigma_1}{E} + \nu \frac{\Delta\sigma_2}{E} + \nu \frac{\Delta\sigma_3}{E}$$

for $\sigma_2 = \sigma_3$ and $\nu = 0.5$, then

$$\varepsilon_1 = \frac{\Delta\sigma_1 - \Delta\sigma_3}{E} + (1 - 2\nu) \frac{\Delta\sigma_3}{E}$$

$$\varepsilon_1 = \frac{\Delta\sigma_1 - \Delta\sigma_3}{E} = \frac{\Delta\sigma_d}{E}$$

Therefore, for a constant Young's modulus (E) with depth, the strain or ε_1 profile has the same shape as the elastic ($\Delta\sigma_1 - \Delta\sigma_3$) variation or Schmertmann's I_z factor (Schmertmann 1970, Schmertmann et al. 1979 and Norris 1986). Taking ε_1 at depth B/2 below the shaft base (the peak of the I_z curve), the shaft base displacement (z_T) is a function of the area of the triangular variation (Fig. 3-9), or

$$z_T = \varepsilon B \qquad (3\text{-}26)$$

Dealing with different values for the pile tip resistance, the associated deviatoric stress (ε) and base movement (a function of strain, ε) can be determined (given the stress-strain, $\sigma_d - \varepsilon$ relationship of the clay immediately below pile tip) in order to construct the pile point load-point displacement curve.

3.5 PROCEDURE VALIDATION

3.5.1 Comparison with the Seed-Reese t-z Curve in Soft Clay (California Test)

The test reported by Seed and Reese (1957) was conducted in the San Francisco Bay area of California. As shown in Fig. 3-10, the soil conditions at that site consisted of 4 ft of

fill, 5 ft of sandy clay, and around 21 ft of organic soft clay “bay mud”. The water table was approximately 4 ft below ground.

Several 6-in.-diameter pipe piles (20 to 22 ft long) were driven into the above soil profile. The pipe pile had a coned tip and maximum load of 6000 lb. The top 9 ft of the nonhemogeneous soil was cased leaving an embedment in clay of 13 ft.

A number of disturbed and undisturbed unconfined compression tests were conducted to determine the unconfined compressive strength of clay (Fig. 3-11). Seven loading tests were performed on the same pile at different periods of time that ranged from 3 hours to 33 days. As shown in Fig. 3-12, the ultimate bearing capacity of the clay reached a stable and constant value (6200 lb) by the time of the seventh test. As a result, Coyle and Reese (1966) considered the results of the seventh load test as representative for stable load transfer-pile movement response.

Coyle and Reese (1966) used the data obtained from the current field test conducted by Seed and Reese (1957) to compute the values of the load transfer response and pile movement at different depths as seen in Fig. 3-13. Figure 3-14 exhibits an equivalent set of the t-z curves at the same depths that are constructed by using the procedure presented herein and based on the undrained compressive strength of clay that is described by the dashed line shown in Fig. 3-11. The good agreement between the experimental and predicted t-z curves can be seen in the comparison presented in Fig. 3-15. Such agreement speaks to capability of the technique presented. The predicted t-z curve at the deepest two points (20 and 22 feet below ground) and seen in Fig. 3-15 can be improved by a slight increase in the undrained compressive strength utilized.

The good agreement between the predicted and experimental t-z curves resulted in an excellent assessment for load distribution (due to shear resistance) along the pile. Fig. 3-16 shows the assessed load distribution and tip resistance that are based on the procedure presented and induced in 1000-lb axial load increments up to an axial load of 6000 lb. A

comparison between the measured and predicted load distributions along the pile is shown in Fig. 3-17.

The measured pile head load-settlement curves under seven cases of axial loads are shown in Fig. 3-18. The loading tests were performed at different periods of time after driving the pile. As mentioned earlier, the seventh test (after 33 days of driving the pile) is considered for the validation of the procedure presented. Reasonable agreement can be observed between the predicted and measured pile head load-settlement curve (Fig. 3-18).

It should be noted that Seed and Reese (1957) established a procedure that allows the assessment of the pile load-settlement curve and the distribution of the pile skin resistance based on the data collected from vane shear test shown in Fig. 3-1. In addition, some assumptions should be made for the point load movement in order to get good agreement with the actual pile response. Seed and Reese (1957) presented explanation for the lack of agreement between their calculated and measured data. The undrained compressive strength collected using the vane shear test was the major source of that disagreement.

3.6 SUMMARY

The procedure to evaluate the t-z and load-settlement curves for a pile in clay presented here is based on elastic theory and Ramberg-Osgood characterization of the stress-strain behavior of soil. This procedure allows the assessment of the mobilized resistance of the pile using the developed t-z curve and the pile point load-displacement relationship. The results obtained in comparison with the field data show the capability and the flexible nature of the suggested technique. Based on the comparison study presented in this chapter, the good agreement between the measured and predicted load transfer along the pile, pile movement, pile-head settlement and pile tip resistance shows the consistency of the technique's assumptions. The findings in this chapter will be employed in Chapter 5 to evaluate the vertical side shear resistance induced by the lateral deflection of a large diameter shaft and its contribution to the lateral resistance of the shaft.

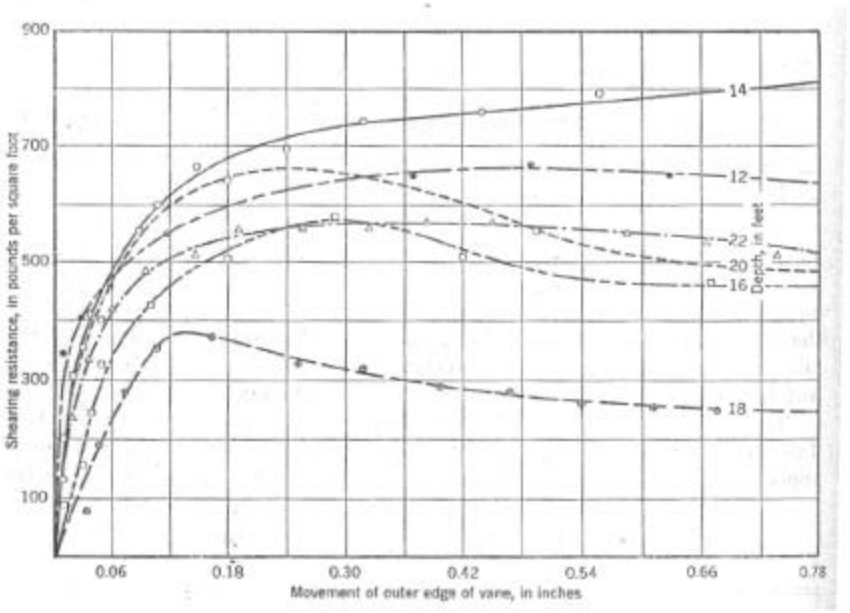

Fig. 3-1 Shear Resistance vs. Movement Determined by the Vane Shear Test (Seed and Reese 1957)

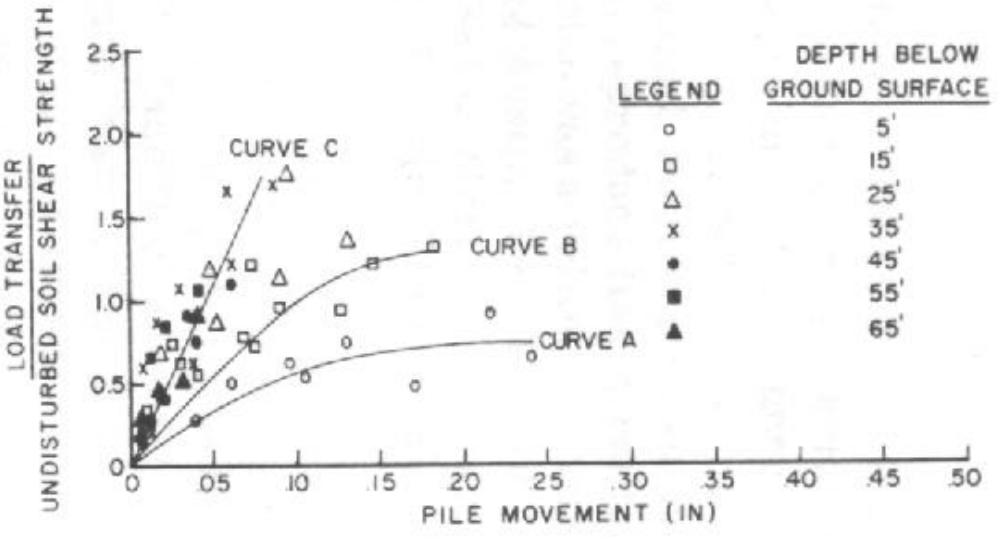

Fig. 3-2 Ratio of Load Transfer to Soil Shear Strength Vs. Pile Movement for a Number of Field Tests (Coyle and Reese 1966)

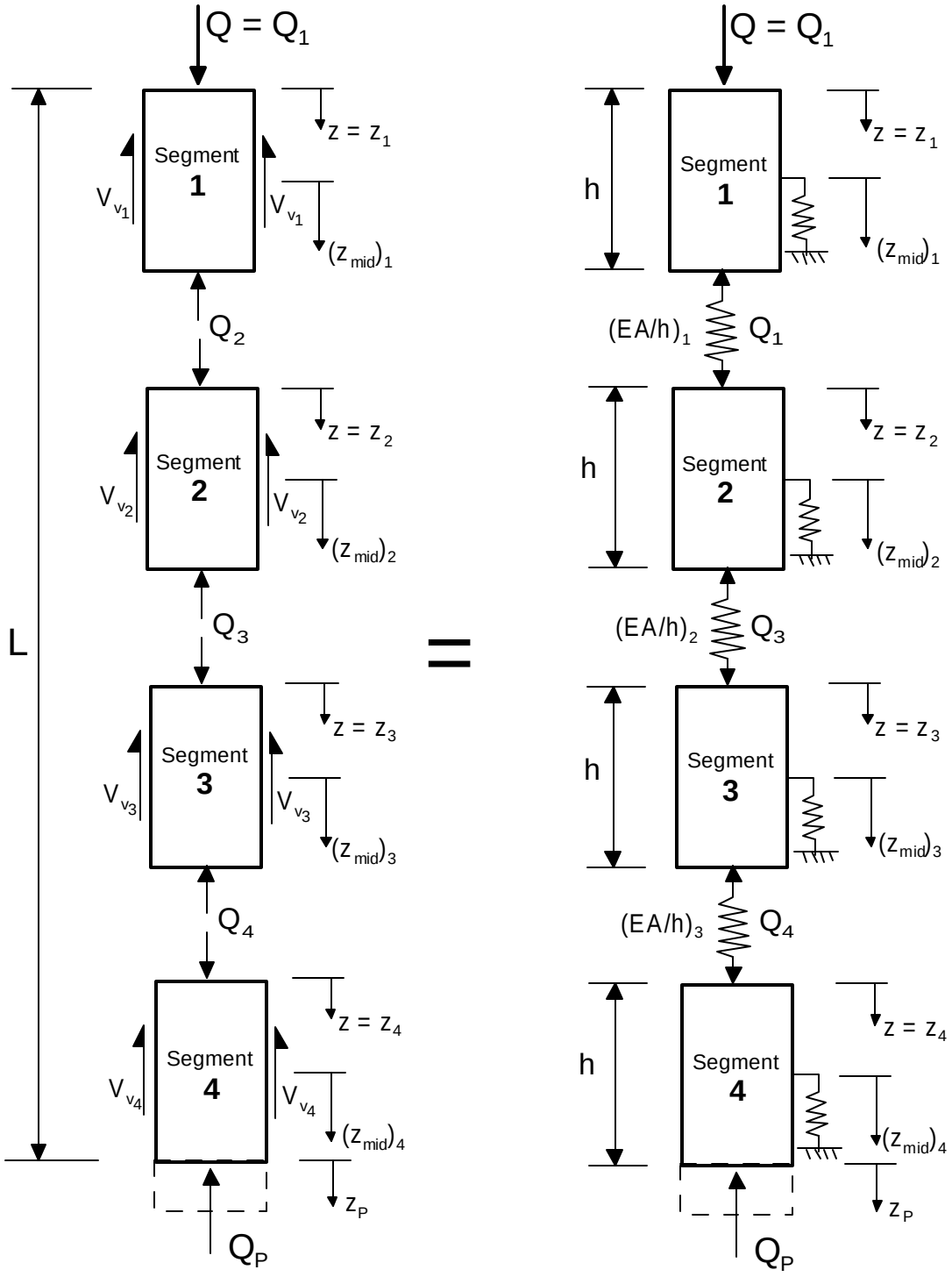

Fig. 3-3 Modeling Axially Loaded Pile Divided into Segments

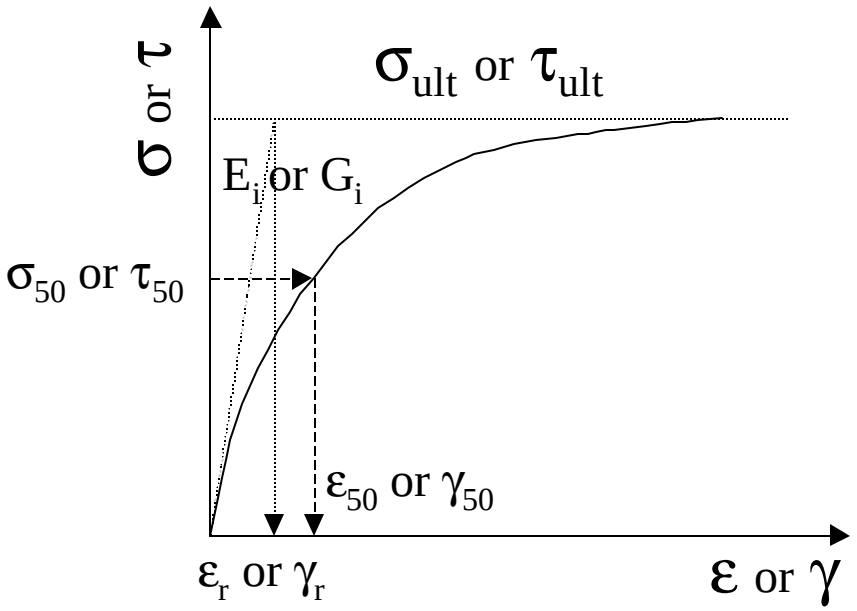

Fig. 3-4 Basic (Normal or Shear) Stress-Strain Curve

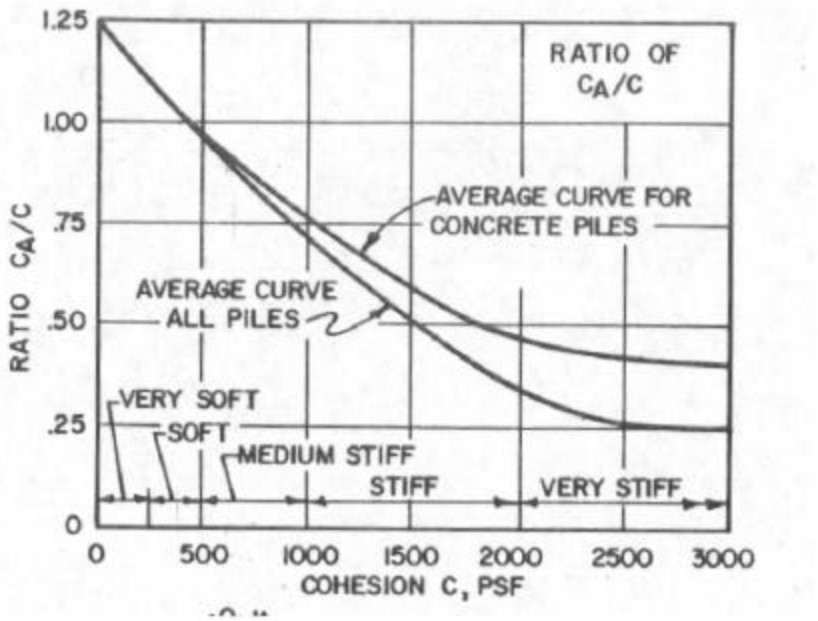

Fig. 3-5 Changes in Clay Cohesion Adjacent to the Pile Due to Pile Installation (DM7.2 1986)

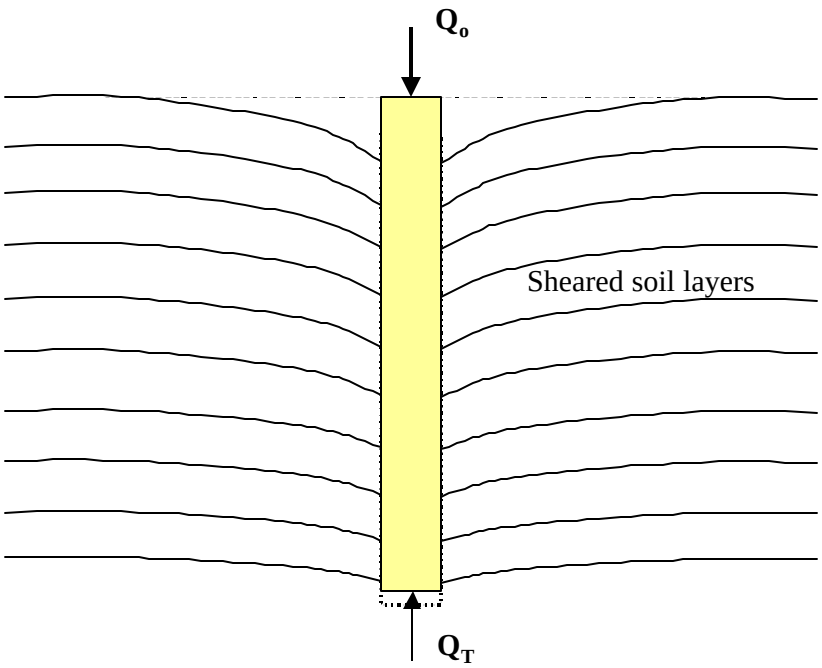

Fig. 3-6 Soil Layer Deformations Around Axially Loaded Pile

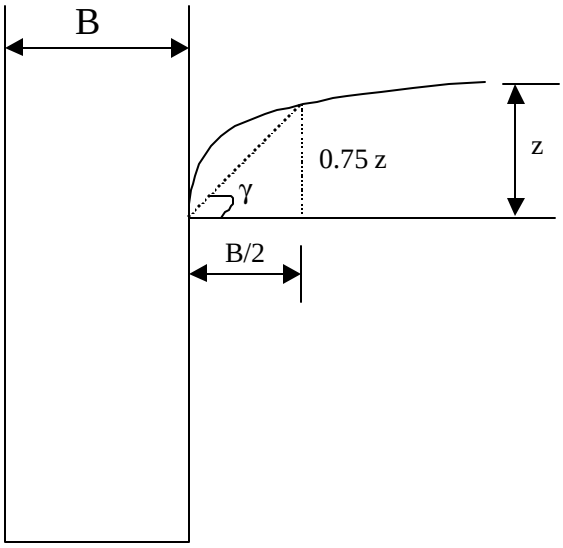

Fig. 3-7 Idealized Relationship Between Shear Strain in Soil (γ) and Pile Displacement (Z) (Norris, 1986)

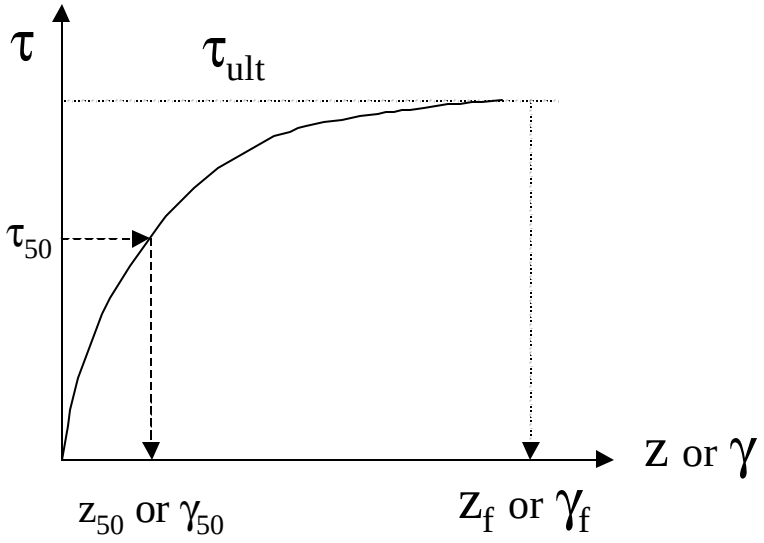

Fig. 3-8 Soil Shear Resistance Vs. Shear Strain (γ) or Pile Movement (z)

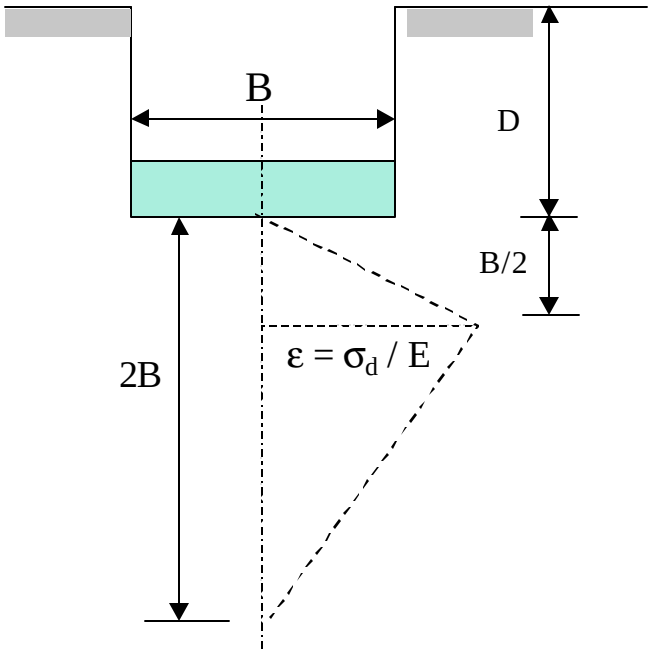

Fig. 3-9 Schmertmann Strain Distribution Below Foundation Base
(after Norris, 1986)

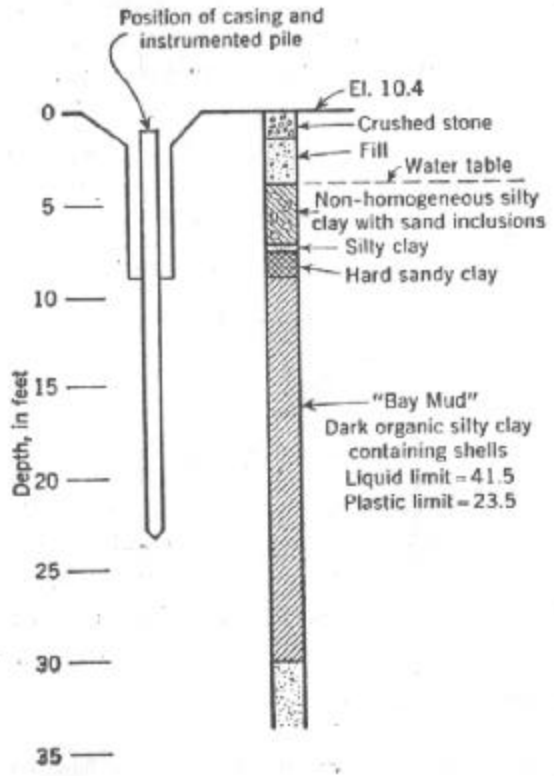

Fig. 3-10 Driven Pile and Soil Profile for California Test (Seed and Reese 1957)

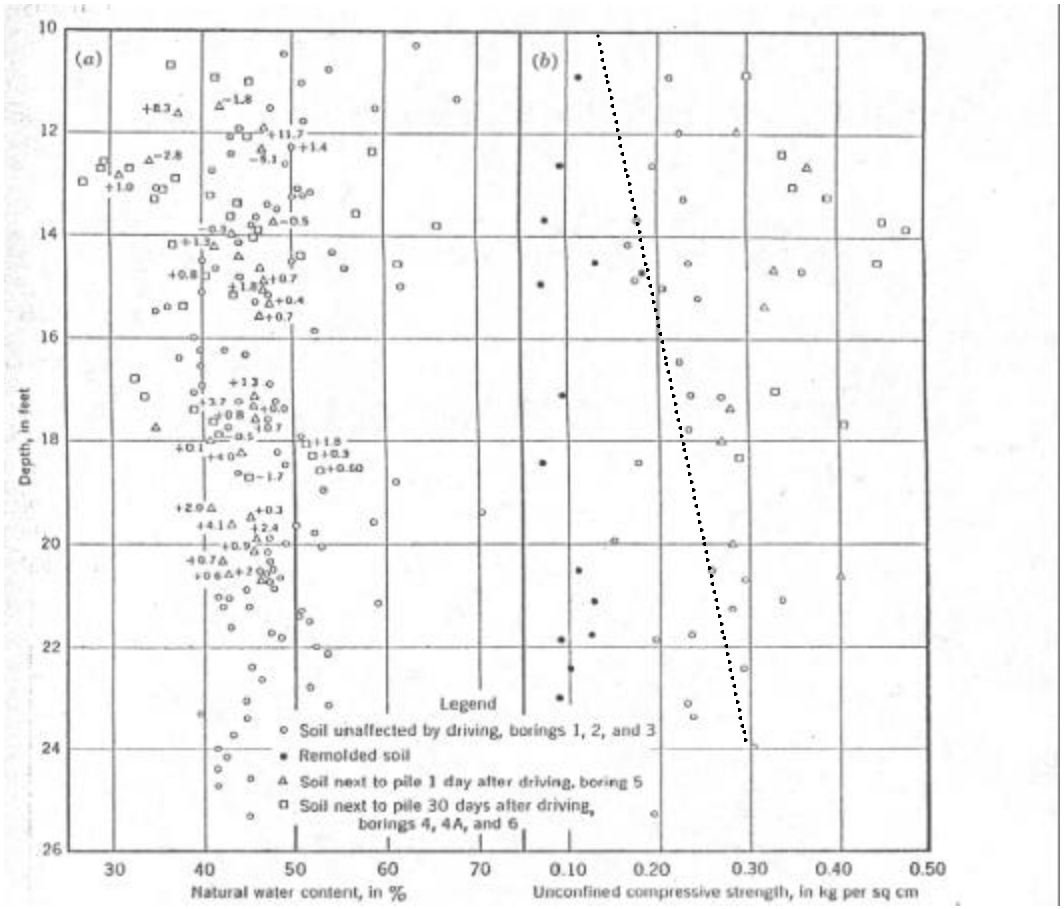

Fig. 3-11 Results of Soil Tests for the Undrained Shear Strength of the Bay Mud in California Test (Seed and Reese 1957)

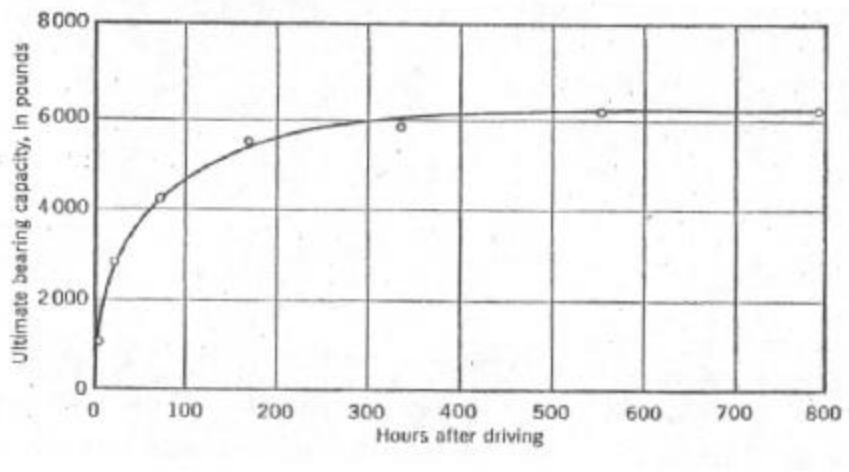

Fig. 3-12 Variation of the Clay Bearing Capacity with Time
(California Test, Seed and Reese 1957)

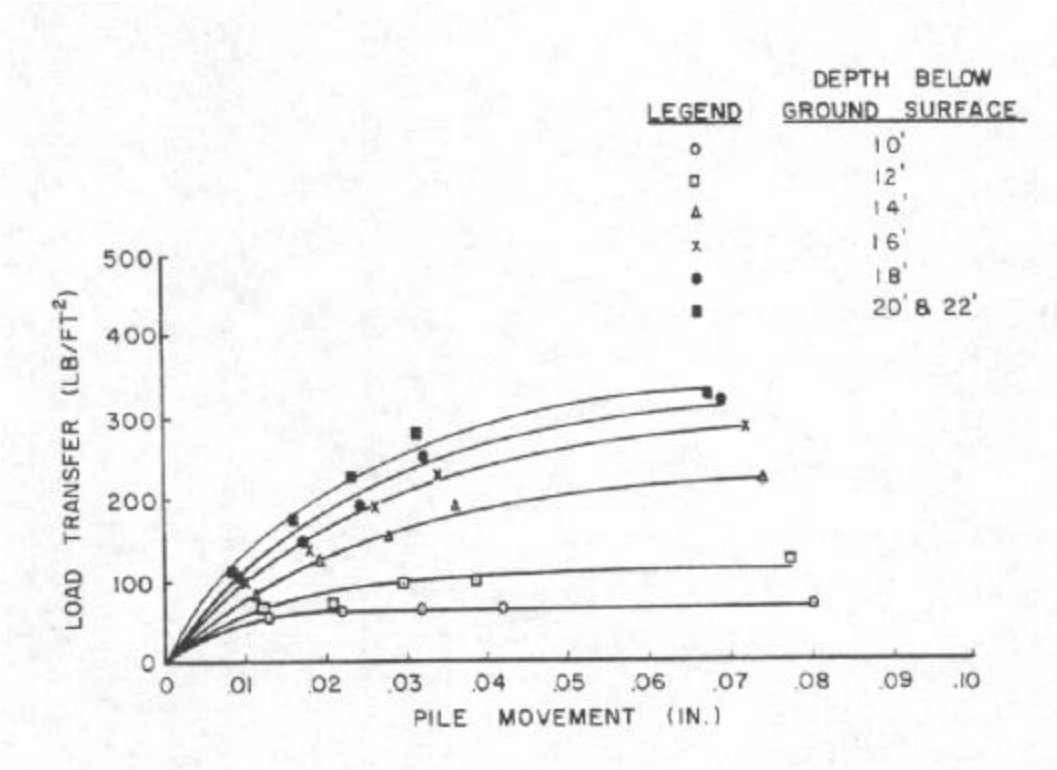

Fig. 3-13 Measured Load Transfer (τ) – Pile Movement (z) Curve for California Test
(Coyle and Reese 1966)

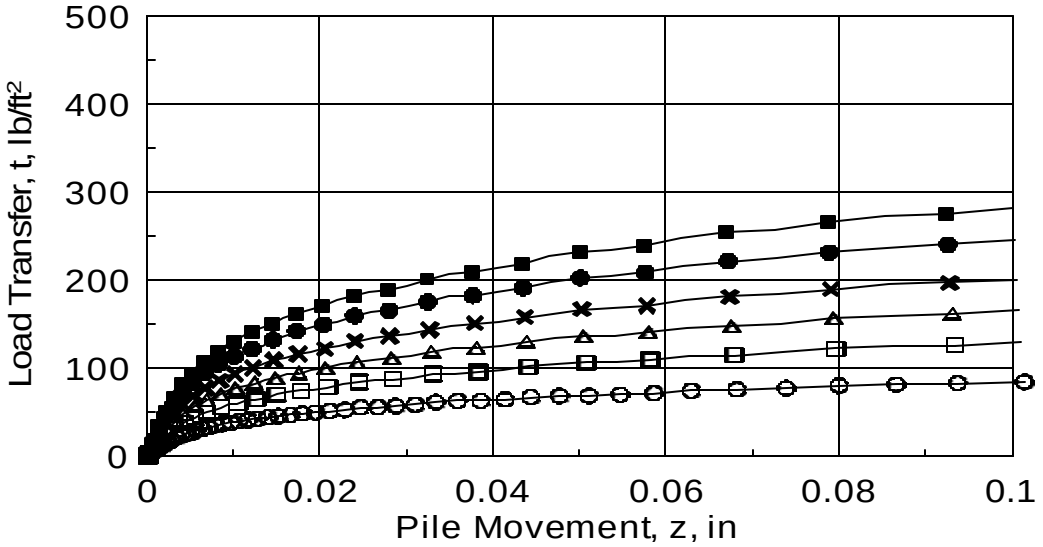

Fig. 3-14 Predicted Load Transfer (τ) – Pile Movement (z) Curve for California Test Using the Suggested Procedure

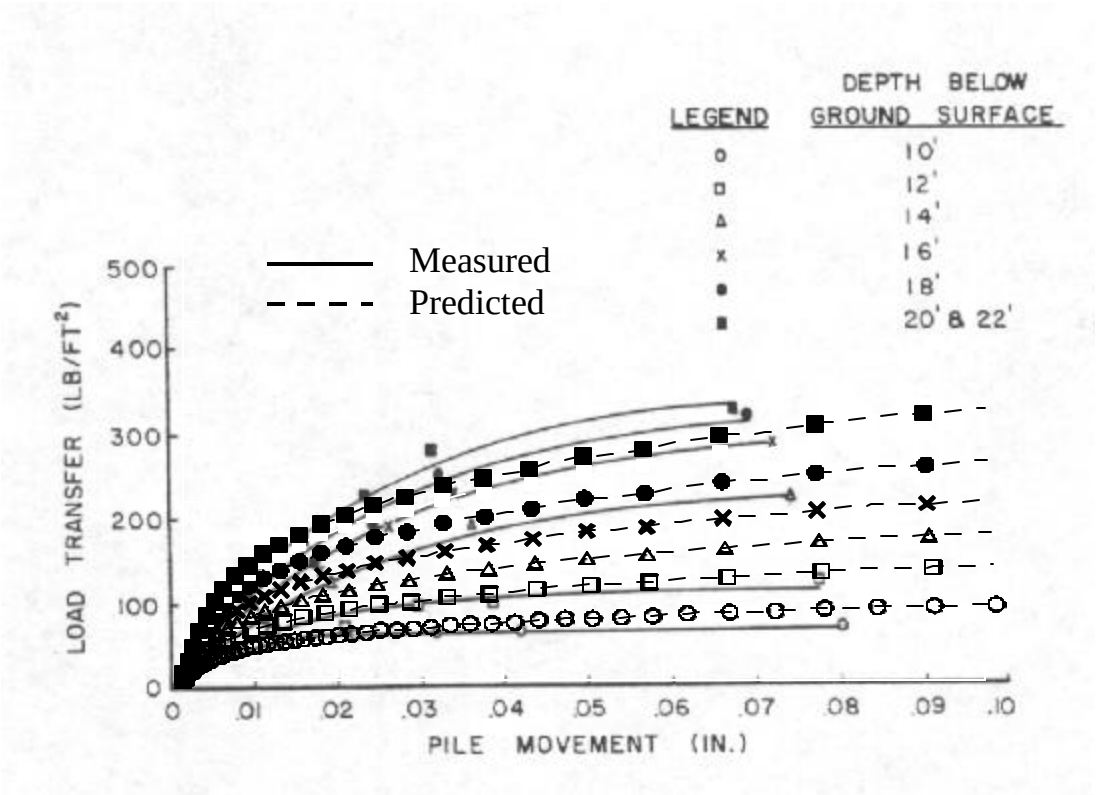

Fig. 3-15 Comparison Between Measured and Predicted Load Transfer (τ) – Pile Movement (z) Curve for the California Test

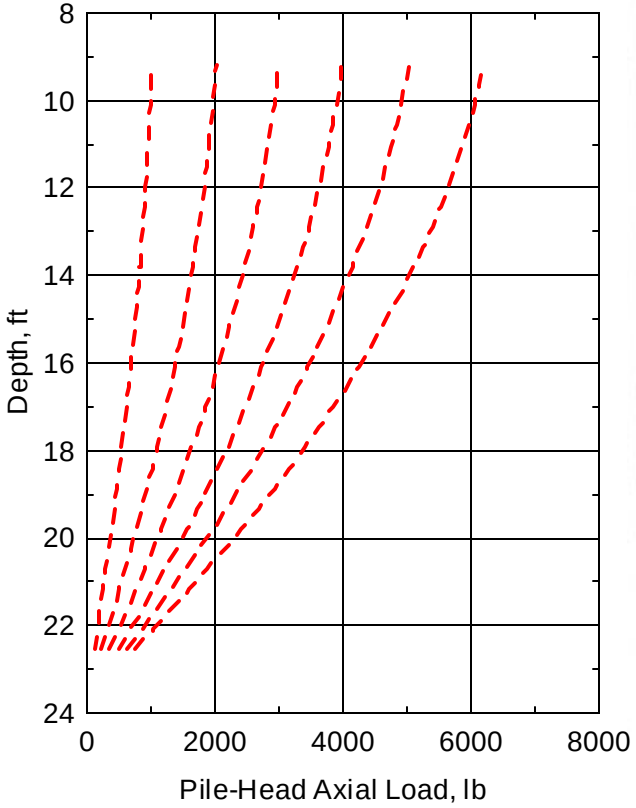

Fig. 3-16 Predicted Load Distribution along the Pile in California Test

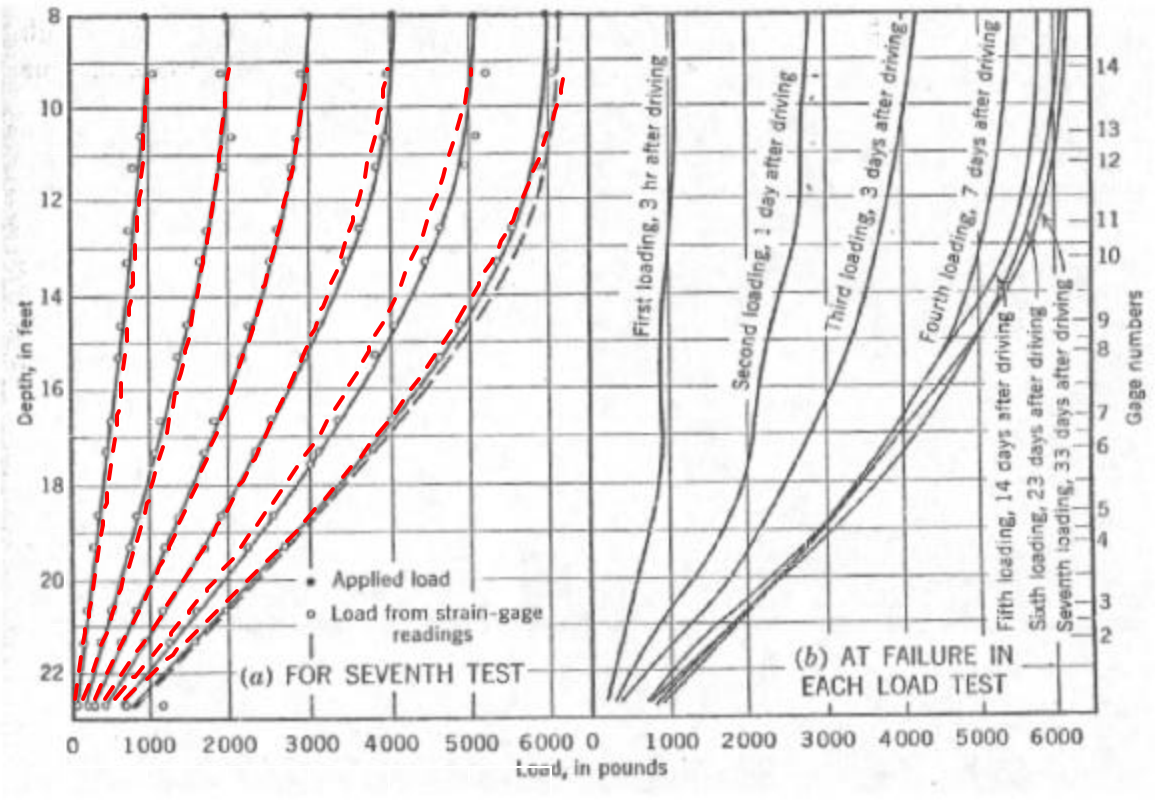

Fig. 3-17 Comparison of Measured and Predicted Load Distribution along the Pile in California Test (Seed and Reese 1957)

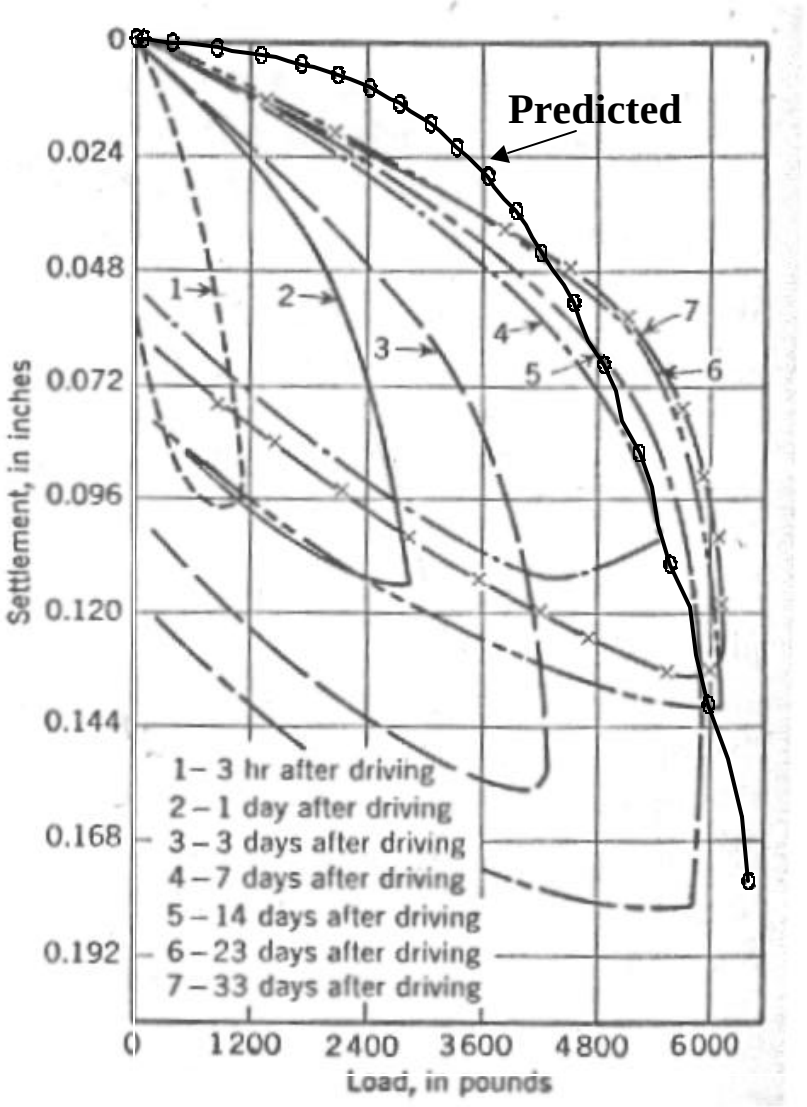

Fig. 3-18 Pile-Head Load-Settlement Curves for Seven Loading Tests at Different Time Periods for the California Test in Comparison with the Predicted Results